Heat and Mass Transfer
https://doi.org/10.1007/s00231-022-03280-5

ORIGINAL

An experimental evaluation of thermoelectric generator performance under cyclic heating regimes

N. P. Williams[1] · J. Power[1] · D. Trimble[1] · S. M. O'Shaughnessy[1]

Received: 2 February 2022 / Accepted: 10 August 2022

Abstract

Thermal cycling is known to adversely affect the performance and lifespan of thermoelectric generators (TEGs) yet has received limited attention to date. The current study experimentally investigates the effect of thermal cycling on the performance of twelve nominally identical TEG modules. Six samples were subjected to the same thermal cycle profile with an average heating time of 154 s to examine the variation in their outputs. The maximum cycling temperature was varied between 170 °C and 190 °C for a further six samples to investigate the effect of maximum set-point temperature on performance. Degradation in performance was exhibited by all modules, with maximum power outputs between 28% and 57% of pre-cycling values and a decrease in the dimensionless figure of merit *ZT* of 21% to 56% upon cessation of cycling. Sudden 'breakdowns' or significant reductions in output power were observed for all TEGs, accompanied by increased electrical resistance, which is indicative of internal damage to the modules arising from the formation of micro-cracks at the interface between the semiconductor thermocouples and electrically conductive material. The rate of degradation post-'breakdown' appeared to be influenced by the maximum set-point temperature, with more rapid decreases observed for increasing temperatures.

Nomenclature

A	Cross-sectional area [m^2]
I	Current [A]
K	Thermal conductance [W/K]
L	Length [m]
Q	Heat power [W]
R	Electrical resistance [Ω]
T	Temperature [°C]
V	Voltage [V]
W	Electrical power [W]
Z	Figure of Merit [1/K]
ZT	Dimensionless Figure of Merit

Greek symbols

α	Seebeck coefficient [V/K]
Δ	Gradient
λ	Thermal conductivity [W/mK]
ρ	Density [kg/m^3]
σ	Electrical conductivity [S/m]

Subscripts

C	TEG cold side
eff	Effective
H	TEG hot side
L	Electrical load
max	Maximum
OC	Open circuit
n	N-type semiconductor
p	P-type semiconductor

1 Introduction

Thermoelectric generators (TEGs) are solid state semiconductor devices which convert heat energy to electrical energy through the Seebeck effect, with wide-ranging applications including vehicle exhaust heat recovery systems [1], low power sensors [2], off-grid electricity generation [3], and wearable technologies [4]. Greater voltages across the electrical terminals of the TEG and higher output power are generated by the module for increasing temperature difference between its hot and cold surfaces while the maximum operating temperature is not exceeded. The absence of moving parts in their construction means that TEGs are often quoted with long lifetimes by manufacturers when assumed to be operating under stable thermo-mechanical conditions. However, their expected lifetimes and output power can

✉ N. P. Williams
nwilliam@tcd.ie

[1] Department of Mechanical, Manufacturing, and Biomedical Engineering, Parsons Building, Trinity College, The University of Dublin, Dublin, Ireland

Published online: 01 September 2022

be significantly reduced when the devices are subjected to thermal cycling, which has received limited attention in literature to date. There appears to be no standard method to impose thermal cycling on TEGs, or to evaluate its effects. Several analytical and/or numerical studies, such as those in Refs. [5–7], have attempted to provide greater insight, but the models are typically limited in their applicability to real life scenarios, and they often do not consider material degradation effects. An exception to this is the study of Wang et al. [8].

Regarding experimental studies, Hori et al. [9] were among the first to examine the effect of thermal cycling on TEG performance, investigating three bismuth telluride (Bi_2Te_3) modules of varying thermoelement cross-sectional area. The hot side was cycled to a maximum temperature of 180 °C, while the cold side was maintained at 30 °C. The duration of the thermal cycle was not detailed. Thermal cycling was found to have a detrimental effect on the TEG modules' performance, attributed to increased internal electrical resistance, with the power generated decreasing over successive cycles. The authors observed a sudden decrease or 'breakdown' in performance for all modules, with greater lifespan linked to increased thermoelement cross-sectional area.

Hatzikraniotis et al. [10] examined the thermal cycling of Bi_2Te_3 TEGs of 25 mm × 25 mm cross-sectional area containing 31 thermoelements. A thermal cycle consisted of a heating stage of approximately 6 min to a hot side temperature of 200 °C, a constant temperature period lasting approximately 5 min, followed by a cooling stage of approximately 20 min to a minimum hot side temperature of 30 °C. The cold side temperature was fixed at 24 °C. At the end of 6,000 thermal cycles, the module experienced a drop in output power of approximately 14% and an increase in material resistivity of 16.1%. The authors attributed this degradation to micro-crack formation at the thermoelement leg/solder interface, as observed through scanning electron microscope (SEM) imaging of the module's internal structure post-cycling. The dimensionless figure of merit *ZT* was also observed to have decreased from 0.74 to 0.63 upon the cessation of cycling. A larger decrease in *ZT* of 18.7% was observed by de Cerqueira Veras et al. [11] who developed a testing platform to investigate thermal cycling effects on a single thermoelectric module. The sample was subjected to temperature differences of ± 20 ℃ in the temperature range of 20 ℃ to 40 ℃, with each cycle lasting 15 minutes. After 548 cycles, the internal resistance, Seebeck coefficient, thermal conductivity, and electrical conductivity changed by + 9.8%, -3.9%, -8.6%, and -9.6%, respectively.

The hot side temperature of a TEG module was varied between -20 °C and 146 °C by Barako et al. [12, 13] through the application of a square wave voltage signal to the module, replicating both heating and cooling cycles. The cold side was maintained at 23 °C using a heat exchanger. Upon completion of 45,000 cycles each lasting 60 s, the cyclable hot side temperature range had decreased to between 20 °C and 40 °C, indicating failure of the module. A decrease in the figure of merit and significantly increased internal resistance was attributed to fracture of the TEG leg/solder interface, detected through infrared (IR) microscopy.

Tatatinov et al. [14] cycled the hot side of a TEG module between 50 °C and 250 °C while maintaining a cold side temperature of 30 °C. For a cycle time of 11 min, the module's output power was observed to have decreased by 11% after 340 cycles, which the authors believed was due to the degradation of the thermal contact at the solder leg and thermoelement interface.

The use of TEG modules as the hot and/or cold side source when thermal cycling an additional TEG has been employed by a number of authors. Park et al. [15] utilised two TEG modules thermally in series as the hot side source for the thermal cycling of a module. Thermal cycles of three-minute duration between temperatures of 30 °C and 160 °C were applied to the module, with the cold side maintained at 20 °C. Decreases of 8% and 11% in the figure of merit and output power respectively were observed after 6,000 cycles. Tenorio et al. [16] alternated the hot and cold sides across a TEG module between 20 °C and 40 °C for thermal cycles lasting approximately 15 min by utilising additional TEG modules as the hot and cold sources. A decrease in *ZT* of 7% after only 127 cycles was observed, with a 10% increase in the internal resistance.

Ding et al. [17] examined the effect of varying thermal cycling conditions on TEG performance, for heat inputs of 80 W and 160 W and heating and cooling times of 15 minutes. This corresponded to the thermal cycling ranges 35 °C to 85 °C and 55 °C to 165 °C respectively. No change in output performance was determined under the first cycling range after 500 thermal cycles. However, when subjected to cycling at the higher hot side temperature, the module's open-circuit voltage exhibited unexpected fluctuations, which was attributed to degradation of the solder connections within the module. The authors concluded that prolonged cycling of TEG modules at hot side temperatures of approximately 150 °C is detrimental to their performance.

Merienne et al. [18] recently investigated the effect of heating rate on three nominally identical Bi_2Te_3 TEGs as produced by a single manufacturer. All samples exhibited performance degradation after 600 thermal cycles, with the greatest degradation experienced by the sample subjected to the most rapid heating rate.

Harish et al. [19] assessed the impact of thermal cycling on eight Bi_2Te_3 modules used in an automotive exhaust thermoelectric generator. Measurements of the open circuit voltage, voltage-current relationship, and matched load output power were obtained in response to three thermal cycling profiles

with a maximum heat source temperature of 350 ℃. After 150 cycles, only marginal variations in the measured parameters were observed. However, after 300 cycles a noticeable decrease in maximum output power was observed for two TEGs which was due to an increase in internal resistance caused by contact resistance at the cold-side leg–electrode joints. Microstructural and compositional analyses indicated that the cold-side joint contact resistance increase arose from the thermochemical degradation of the interface between the thermocouple legs and Sn-Cu solder alloy.

Ziolkowski et al. [20] investigated the short-term (60 h) and long-term (443 h) stability of four TEG samples from different manufacturers using thermal cycling between a fixed cold side temperature of 50 ℃ and hot side temperatures varying between 100 ℃ to 200 ℃ and 125 ℃ to 225 ℃ depending on the sample studied. Tests were conducted at an applied pressure of 3 MPa and long-term stability was assessed on the basis of the internal electric resistance. Internal resistance changes of 2.43%, 4.3%, 13.1%, and 9.16% were obtained for the samples identified as A, B, C, and D, respectively.

Riyadi et al. [21] used a similar experimental setup to Merienne et al. [18] to thermally cycle an SP1848 27145 SA TEG for 100 cycles at four heating rates: 3.92 ℃/s, 2.67 ℃/s, 1.64 ℃/s, and 0.91 ℃/s. The average temperature difference during thermal cycling was 110 ℃ for all tests. An increasing number of thermal cycles led to an increase in TEG internal resistance and a corresponding decrease in output voltage, current and power, with greater deterioration at higher heating rates. Lower heating rates resulted in an increase in the Seebeck coefficient.

Clearly, thermal cycling has a deleterious effect on TEG performance, at least at the macro scale. Although not within scope of this study, with the advent of thin film TEGs and newer organic and inorganic thermoelectric materials, further work is required to assess robustness and reliability over repeated thermal cycles. For example, Mirhosseini et al. [22] thermally cycled a zinc antimonide (Zn-Sb) thin film thermoelectric sample, subjecting the sample to different thermal gradients. They observed no deterioration in performance; however, only 10 cycles each of 8 min duration were conducted. Other studies have been performed to mitigate thermal cycling effects through, for example, protective coatings [23]. Gao et al. [24] used nanostructured interfaces based on vertically aligned carbon nanotubes (CNT) to simultaneously address the issues of mechanical stability and large temperature drops in thin film TEGs. They subjected their thin film sample to 100 thermal cycles from 30 ℃ to 200 ℃, finding no significantly detrimental effect on the CNT array, whilst acknowledging the need for further studies and sample imaging before and after cycling.

A summary of the studied parameters from several pertinent TEG thermal cycling studies is provided in Table 1. There are differences in the number of TEGs investigated per study, the TEG size and number of p-n pellets, the pellet length and cross-sectional area, the temperature limits imposed, and the duration and number of thermal cycles performed. This leads to differing results. A greater understanding of thermal cycling effects on commercially available modules is required to ensure their sustainable application. In this work, two distinct investigations were undertaken to examine the impact of the operating conditions on the performance degradation of TEG modules. In the first study, six TEG samples produced by a single manufacturer were subjected to the same thermal cycling profile to examine the variation in performance between nominally identical samples under the same conditions. In the second study, a further six TEG samples from the same manufacturer were subjected to different maximum temperature limits during thermal cycling to determine the effect on module degradation. To the authors' knowledge, this represents the largest number of TEG samples, particularly from a single manufacturer, investigated in a single study.

2 Thermoelectric theory

Under the Seebeek effect, when conductors of dissimilar material are subjected to a thermal gradient, the diffusion of charge carriers across this temperature difference develops an electrical potential between the hot and cold ends. This open-circuit voltage V_{OC} can be described in terms of the thermal gradient $\Delta T = T_H - T_C$ and the material's Seebeck coefficient, α, which is the difference between the Seebeck coefficients of the individual semiconductor materials, as given by Eq. (1):

$$V_{OC} = \alpha \Delta T = \alpha (T_H - T_C) \tag{1}$$

TEG modules consist of several p-n semiconductors known as thermoelements or thermocouples connected electrically in series and thermally in parallel. These thermocouples are connected to an electrical shunt such as copper to conduct the current generated and placed between ceramic plates of high thermal conductivity but low electrical conductivity. The efficiency of a thermoelectric device in converting heat energy to electrical energy is dependent upon the thermoelectric material properties. Desirable properties of a thermoelectric material include low thermal conductivity to maintain a thermal gradient across the device, a high electrical conductivity to avoid electron scattering, and a high Seebeck coefficient. A thermoelectric material's performance can be characterised by its figure of merit, Z, as given by Eq. (2) where σ and λ are the material's electrical and thermal conductivity respectively:

Table 1 Summary of pertinent TEG thermal cycling studies

Author(s)	Year	Cycle Length [s]	No. Thermal Cycles [-]	Temperature Limits [°C]	TEG Dimensions [mm^3]	No. of Thermocouples	Number/Type
Hori et al. [9]	1999	–	50 – 300	30 to 180	47.5×47.5×5	49	6×Bi_2Te_3
Hatzikraniotis et al. [10]	2009	1,800	6,000	30 to 200	25×25×3	31	1×Bi_2Te_3
Barako et al. [12, 13]	2012	60	45,000	23 to -20 23 to 146	–	–	–
Tatarinov et al. [14]	2012	–	340	30 to 250	–	–	1×Bi_2Te_3
Park et al. [15]	2012	180	6,000	30 to 160	39.7×39.7×4.16	127	1×Bi_2Te_3
de Cerqueira Veras et al. [11]	2015	900	548	20 to 40	40×40×3.3	127	1×Bi_2Te_3
Ding et al. [17]	2016	1,800	300 – 500	35 to 85 55 to 165	40×40×2.3	127	1×Bi_2Te_3
Tenorio et al. [16]	2017	900	127	20 to 40	40×40×3.9	127	1×Bi_2Te_3
Merienne et al. [18]	2019	760 – 1,320	600	50 to 165	40×40×3.3	127	3×Bi_2Te_3
Williams et al. [25]	2021	990	600	50 to 165	40×40×3.4	127	6×Bi_2Te_3
Harish et al. [19]	2021	960 – 1,320	150 – 300	50 to 300 50 to 350	40×40×5	126	8×Bi_2Te_3
Ziolkowski et al. [20]	2021	155 – 1,230	3 – 151	50 to 200 50 to 225	40×40×3.5 51.5×51.5×4.5 54×54×3.4 50×50×3.5	–	4×Bi_2Te_3
Riyadi et al. [21]	2022	334 – 378	100	30–38 to 163.8 30–38 to 158.3 30–38 to 156.5 30–38 to 155.3	40×40×3.9	110	4×Bi_2Te_3
Current study	2022	940 – 1,061	300 – 750	50 to 165 50 to 170 50 to 180 50 to 190	40×40×3.4	127	12×Bi_2Te_3

$$Z = \frac{\alpha^2 \sigma}{\lambda} \tag{2}$$

The highest figures of merits are observed for TEGs consisting of bismuth telluride thermocouples, with Z values of approximately 3.4×10^{-3} K^{-1}. However, they are limited to maximum operating temperatures of approximately 250 °C. The internal electrical resistance R and thermal conductance K of a single thermocouple can be defined simply in one-dimension according to the standard model proposed by Hodes [26], which defined these properties in terms of the material density (ρ), thermal conductivity, thermocouple length (L) and cross-sectional area (A), as shown in Eqs. (3) and (4):

$$R = \frac{2\rho L}{A} \tag{3}$$

$$K = \frac{2\lambda A}{L} \tag{4}$$

Assuming one-dimensional conduction through the module, the rate of heat absorbed (Q_H) and rejected (Q_C) can be described as:

$$Q_H = K\left(T_H - T_C\right) + \left(\alpha_p - \alpha_n\right) I T_H - \frac{RI^2}{2} \tag{5}$$

$$Q_C = K\left(T_H - T_C\right) + \left(\alpha_p - \alpha_n\right) I T_C + \frac{RI^2}{2} \tag{6}$$

α_p and α_n are the respective Seebeck coefficients of the p and n-type doped semiconductor materials and I is the current through the thermocouple. The electrical power (W) generated by the thermocouple can be expressed as the product of the current through and voltage (V) across the thermocouple. Applying an energy balance across the module, the electrical power can also be expressed as the difference between the heat absorbed and rejected:

$$W = IV = Q_H - Q_C \tag{7}$$

Combining Eqs. (5), (6) and (7):

$$W = I\left(\alpha_p - \alpha_n\right)\left(T_H - T_C\right) - I^2R \tag{8}$$

The thermocouple's voltage at a fixed temperature difference $\Delta T = T_H - T_C$ can be determined by dividing Eq. (8) by the electrical current and combining the Seebeck coefficients into a single parameter $\alpha = \alpha_p - \alpha_n$:

$$V = \alpha\Delta T - IR \tag{9}$$

To measure α, the TEG is subjected to open-circuit conditions and the applied temperature gradient and corresponding voltage is measured. By setting the electrical power W equal to the external load's electrical power I^2R_L in Eq. (8), the thermocouple's current can be described by Eq. (10), where R_L is the load resistance:

$$I = \frac{\alpha(\Delta T)}{R + R_L} \tag{10}$$

Combining Eqs. (9) and (10) provides the thermocouple's power as a function of load resistance and internal resistance for a given temperature difference:

$$W = (\alpha\Delta T)^2\left(\frac{R_L}{\left(R + R_L\right)^2}\right) \tag{11}$$

The maximum power (W_{max}) generated by the thermocouple occurs when the internal resistance matches the resistance of the external load:

$$W_{max} = \frac{(\alpha\Delta T)^2}{4R} = \frac{A(\alpha\Delta T)^2}{8\rho L} \tag{12}$$

From Eq. (12) for a particular thermoelectric material and fixed temperature difference, the thermocouples within the TEG module should be of the shortest length possible with the largest cross-sectional area that can be achieved to obtain the greatest output power.

3 Experimental method

Figure 1 illustrates the experimental set-up employed, which is comparable to that of Merienne et al. [18]. Two aluminium blocks are utilised as the hot and cold sources, between which a single TEG module is placed. The set-up can accommodate TEG modules of cross-sectional areas up to 56×56 mm^2. The upper hot block is provided with the required heat input by two cartridge heaters of 16 mm outside diameter connected to an Elektro-Automatik EA-PSI 8360-10 T power supply. Cooling water at a constant temperature and flow rate from a recirculating chiller provides the necessary cooling to the lower cold block. A Thermo Fisher Scientific Accel 500 LC recirculating chiller was employed during the first study, while an S&A CW-5200 recirculating chiller was utilised to provide the cooling requirements for the second study. The entire test section is insulated with DURATEC-750 calcium silicate insulation of 25 mm thickness to minimise heat loss. The TEG module under test is clamped between the heating and cooling blocks to reduce thermal contact resistance, which is known to affect module performance. Clamping pressure is applied to aluminium plates at each end of the test section. These plates are connected by four M6 bolts of 150 mm length. An adjustable torque screwdriver is used to apply the necessary torque of 0.5 Nm to each bolt, which corresponds to the TEG module's maximum operating pressure of 1.2 MPa. Conical or Belleville spring washers are arranged on each bolt to maintain this pressure during thermal cycling. The surface temperatures on either side of the TEG are approximated from the averaged measurements of two calibrated 1.5 mm diameter K-type

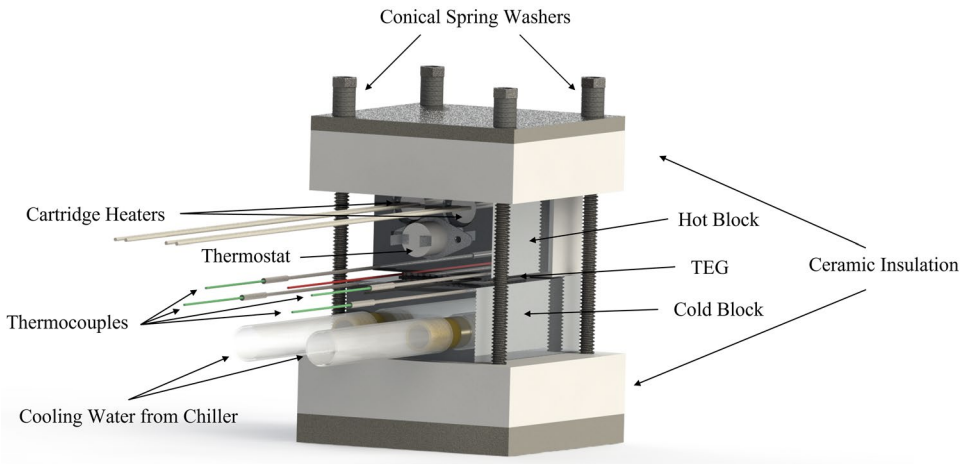

Fig. 1 Rendered CAD image of the experimental test set-up

thermocouple probes placed 1.5 mm from the module's surfaces. These temperature measurements are recorded through a National Instruments (NI) 9211 data acquisition module (DAQ). The maximum uncertainty in the temperature difference measurements in this study is ± 0.27 °C. As a safety measure, a bi-metallic thermostat installed in the upper hot block prevents the temperature exceeding 200 °C. It should be noted that the actual temperature difference experienced by the semiconductor pellets in the TEGs will be lower than that measured in the experiment due to various contact resistances.

During thermal cycling, the power generated by the TEG module is consumed by an Elektro-Automatik EA-EL 9080-45 T electronic load in constant current mode. The output voltage of the module is recorded using an NI-DAQ 9215, a 16-bit analog-to-digital converter (ADC) with a range of ± 10 V and an uncertainty of 0.02% of reading at room temperature. The module's current is indirectly recorded by measuring the voltage drop across a 0.04 Ω ± 1% sense resistor via an NI-DAQ 9219, a 24-bit ADC with a range of ± 125 mV and an uncertainty of 0.1% of reading at room temperature, resulting in a current reading with maximum uncertainty of ± 0.02 A, and a power measurement maximum uncertainty of ± 1.1%.

The experimental results uncertainty arises from the measured parameters of temperature, electrical resistance, and voltage. In accordance with the study of Huang et al. [27], if the experimental result R is a function of small variations of n independent variables, v_i, the uncertainty (w_R) can be expressed as:

$$w_R = \sqrt{\sum_{i=1}^{n} \left(\frac{\delta R}{\delta v_i} \right)^2 \left(\delta v_i \right)^2} \tag{13}$$

All calibrated DAQ modules are connected to the NI LabVIEW programme via an NI-cDAQ 9174 chassis. The heater block and chiller set-point temperatures are PID controlled through state machine architecture employed by a LabVIEW virtual instrument (VI) to regulate the heating and cooling times, with the Ziegler-Nichols tuning method implemented to determine the parameters of the PID control.

The TEG modules investigated in this study were manufactured by European Thermodynamics, model GM250-127–14-10, with a cross-sectional area of 40 × 40 mm^2 and containing 127 thermocouples. The properties of the modules are summarised in Table 2.

All TEG samples were subjected to three performance evaluation tests to examine the effect of the thermal cycling on their output parameters. Under the Harman test, the material properties of the module can be non-destructively evaluated both pre- and post-cycling. When supplied with a small direct current (DC), a small temperature gradient is generated across the module due to the Peltier effect, as well as a voltage difference across the terminals. This voltage is comprised of a resistive heating component V_{Joule} and a Peltier effect-induced temperature difference component $V_{Seebeck}$ [28]. The dimensionless figure of merit ZT at ambient temperature can be determined from Eq. (14).

Table 2 European Thermodynamics (GM250-127–14-10) Bi_2Te_3 TEG module properties for a hot side temperature of 250 °C and a cold side temperature of 30 °C

Parameter	Value
Dimensions	40 × 40 × 3.4 mm^3
Number of thermocouples	127
Maximum hot side temperature	250 °C
Maximum cold side temperature	175 °C
Open circuit voltage	9.93 V
Matched load output voltage	4.96 V
Matched load output current	2 A
Matched load resistance	2.49 Ω ± 15%
Matched load output power	9.9 W

$$ZT = \frac{V_{Seebeck}}{V_{Joule}} \tag{14}$$

Under the Harman test, the TEG is connected to an external power supply providing a constant 10 mA DC current. Upon reaching a stable voltage output, the power supply is switched off and the voltage decay is observed until the module reaches thermal equilibrium. As illustrated in Fig. 2(a), V_{Joule} is determined as the difference between the exponentially decaying Seebeck voltage and the steady-state voltage. The test must be conducted outside of the experimental set-up and therefore can only be performed pre- and post-cycling. The test is performed at least ten times for each TEG sample and the average is taken for the estimated value of ZT.

The characterisation test evaluates the performance of each TEG module before the initiation of thermal cycling and after every 50 thermal cycles by maintaining a fixed temperature difference across the module and increasing the electronic load's current draw from 0.5 A to 1.6 A. Joule heating is induced by this variation in current, with the hot side temperature maintained at ± 2 °C of the desired set-point. During the first study, the hot side was cycled between 50 °C and 165 °C for all modules with the cold side temperature fixed at 30 °C. For the investigation of the influence of maximum cycling temperature, hot side set-point temperatures of 170 °C, 180 °C and 190 °C were applied, with the cold side temperature fixed at 25 °C. Two

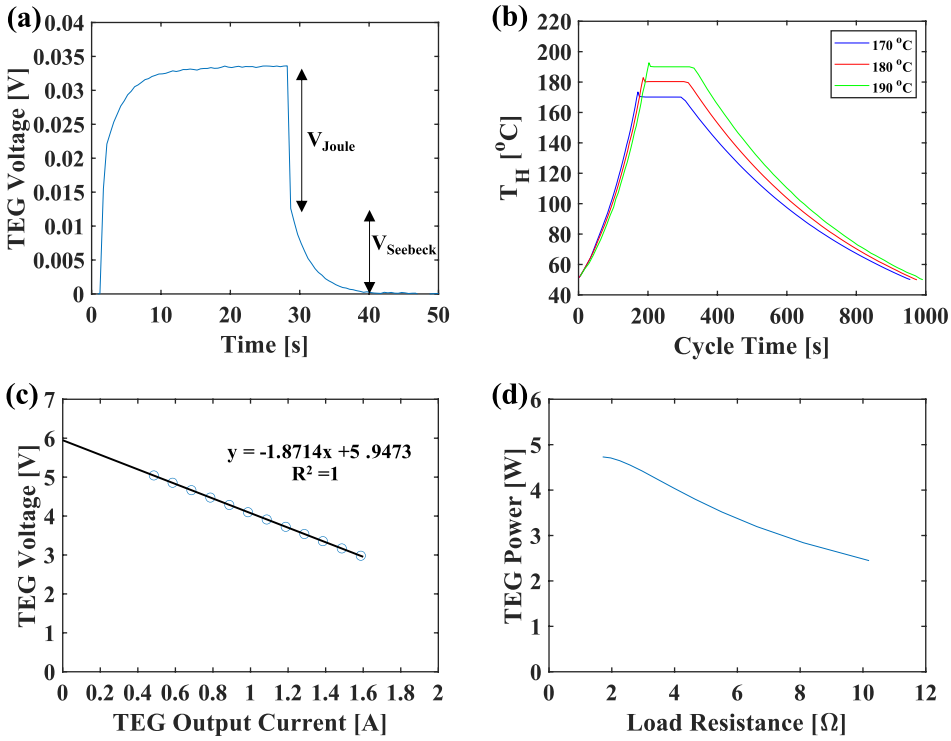

Fig. 2 (**a**) Example of a TEG voltage response during Harman test (**b**) Thermal cycle profiles for maximum hot side temperature investigation (**c**) Determination of TEG open circuit voltage V_{OC} and internal resistance R from the characterisation test, and (**d**) TEG output power pre-thermal cycling as a function of electronic load resistance R_L

samples were tested at each temperature set-point. The heating profile for each of these set-point temperatures is illustrated in Fig. 2(b).

The TEG open circuit voltage V_{OC} can be determined as the y-intercept from a plot of TEG voltage against current, while the internal resistance R is taken as the modulus of the gradient of a line of best fit applied to the data, as illustrated in Fig. 2(c). The maximum TEG output power W_{max} in Fig. 2(d) occurs when the resistances of both the module and electronic load are equal. As detailed by Hsu et al. [29] for real test conditions, the effective Seebeck coefficient α_{eff} can be determined as the ratio of the open circuit voltage of the TEG V_{OC} and the temperature difference maintained across the module's surfaces:

$$\alpha_{eff} = \frac{V_{OC}}{T_H - T_C} \tag{15}$$

Under the conditions of the thermal cycling test, the hot side of the TEG is cycled between 50 °C and the required maximum set-point temperature, under a constant current draw of 1.4 A. Upon reaching the set-point temperature, the desired temperature difference is maintained for at least 60 s to account for fluctuations arising from the Peltier, Joule, and Thomson effects. The voltage and current of both the TEG module and electronic load are recorded, as well as the heating time required to meet the set-point. Upon reaching user defined limits for the hot side mean temperature (< 0.3 ℃) and its standard deviation (< 0.1 ℃), the cooling phase of the thermal cycle is initiated. The average duration of the thermal cycle profiles employed during the investigation, including the average heating and cooling times, are summarised in Table 3. As a safety precaution, and due to the automation of the testing procedure, testing ceased when the maximum power generated by the TEG fell below half of its pre-cycling output. This automation was implemented to mitigate against the TEG recovery effect when thermal cycling is interrupted, as observed by Merienne et al. [18].

Table 3 Thermal cycle profile parameters

Maximum Cycle Temperature [°C]	Average Heating Time [s]	Average Heating Rate [°C/s]	Average Cooling Time [s]	Average Cooling Rate [°C/s]	Total Cycle Duration [s]
165 (TEGs 1 – 6)	154	0.75	660	0.17	940
170 (TEG 7, 8)	169	0.71	691	0.17	984
180 (TEG 9, 10)	182	0.71	699	0.19	1016
190 (TEG 11, 12)	205	0.68	734	0.19	1061

4 Results

4.1 Single set-point temperature study

Characterisation and thermal cycling test results for all samples investigated during the single set-point temperature study are presented in Fig. 3. The normalised maximum output power ($W_{max,norm}$) of the TEGs and their normalised internal electrical resistance (R_{norm}) are presented relative to their pre-cycling values. Table 4 summarises the modules' pre- and post-cycling characteristics, including the *ZT* values as determined from the Harman test. Despite nominally identical properties for all samples with very similar *ZT* values pre-cycling for TEGs 1–5, significant variation in their performance characteristics was determined. As illustrated in Fig. 3(a) decreasing maximum output power was observed as the number of thermal cycles increased, as expected. Furthermore, rapid decreases in output power were experienced by all samples, in line with the 'breakdown' in performance as outlined by Hori et al. [9]. However, despite their similar characteristics pre-cycling, the TEG modules experienced this event at varying cycle numbers. The maximum power generated by TEG 2 was significantly reduced after only 200 cycles, with the minimum power threshold of 50% reached after 350 cycles. More extreme behaviour was exhibited by TEG 3 and TEG 5, with reduced output power of 14% and 30% after 150 cycles and 200 cycles respectively. Thermal cycling ceased for both samples after 300 cycles. More gradual power reductions were observed for TEG 1, TEG 4 and TEG 6, with 'breakdown' occurring after 300, 350 and 450 cycles respectively. The substantial increase in the modules' internal resistance as shown in Fig. 3(b) and decreased effective Seebeck coefficient of Fig. 3(c) corresponding to these 'breakdown' events may be indicative of internal structural damage through the formation of micro-cracks at the interface between the thermocouples and the conductive copper substrate, in line with the findings of Hatzikraniotis et al. [10]. Damage to the TEG's structure as a result of thermal cycling was investigated through microscopic imagery of the leg-solder interface, as illustrated in Fig. 4. The formation of a crack in a thermocouple leg of TEG 5 is evident, emanating from the soldered connection at the copper substrate and propagating toward the opposing leg-solder interface. More substantial damage post-thermal cycling was observed in TEG 6, with through-thickness fracture of a thermocouple leg resulting in the failure of the entire TEG. Further indication of the damage to the internal structure of the TEGs because of thermal cycling was the inability of the electronic load to draw the maximum set-point current from the module during the final characterisation test performed. Reductions in *ZT* were determined for TEGs 1–5 upon completion of thermal cycling, dominated by

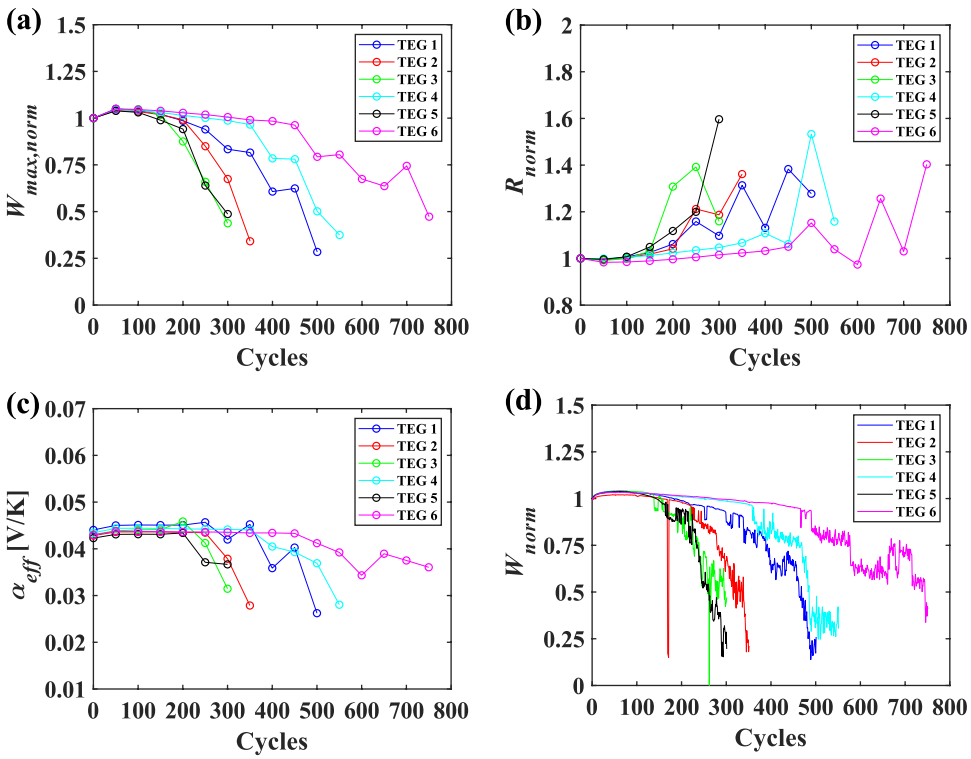

Fig. 3 Performance of all TEG samples from the single set-point temperature investigation characterisation tests including (**a**) normalised maximum output power (**b**) normalised internal electrical resistance (**c**) effective Seebeck coefficient and (**d**) normalised output power from the thermal cycling test

Table 4 Characteristics of the TEG samples investigated for the single set-point temperature study. Maximum uncertainties for each parameter are presented

	Pre-cycling					Post-cycling		
	V_{OC} [V] ±0.02%	α_{eff} [V/K] ±0.17%	R_{pre} [Ω] ±1.2%	W_{max} [W] ±1.1%	ZT_{pre} ±1.4%	ZT_{post} ±1.4%	$ZT_{decrease}$	R_{post} [Ω] ±1.2%
TEG 1	5.95	0.0440	1.87	4.73	0.594	0.303	49%	2.39
TEG 2	5.78	0.0428	1.90	4.40	0.580	0.416	28%	2.59
TEG 3	5.81	0.0430	1.95	4.34	0.597	0.471	21%	2.54
TEG 4	5.86	0.0434	1.90	4.53	0.596	0.342	43%	2.20
TEG 5	5.72	0.0423	2.03	4.03	0.602	0.359	40%	3.25
TEG 6	5.83	0.0430	2.01	4.21	–[a]	0.079	–	2.83

[a]Value for ZT_{pre} unavailable due to hardware failure

the increased Joule voltage V_{Joule} arising from the rise in the TEG modules' internal electrical resistance. TEG 1 was found to have experienced the greatest *ZT* decrease of 49%. A hardware failure prevented the determination of a *ZT* value for TEG 6 pre-cycling; however, the substantial degradation of this module was evident from the low value post-cycling.

This degradation in performance is further apparent from the modules' output power during thermal cycling, normalised by the output power recorded after the first thermal cycle, as shown in Fig. 3(d). All samples exhibited reduced output as cycling increased, in line with the results of their respective characterisation test. Upon occurrence of performance 'breakdown', fluctuations in output power between successive cycles were observed as the module's internal structure deteriorated. For TEG 1 and TEG 4, the output power appeared to stabilise after the initial 'breakdown' point, before experiencing additional material damage and further decreases in performance. In contrast, both TEG 2 and TEG 5 experienced continuous deterioration in their output after the initial performance drop. Reductions in the heating time required for all modules to reach their set-point temperature were observed for increasing thermal cycle number, which we believe to be indicative of lower material thermal conductivity resulting from internal crack formation. The normalised power output for both TEG 2 and TEG 3 approached zero during a single cycle during thermal cycling as a result of poor electrical connections to the DAQ module. Upon rectification, they returned to values in line with their preceding and proceeding cycles.

4.2 Maximum cycle temperature study

Figure 5 presents the results from the characterisation and thermal cycling testing of all samples (TEGs 7—12) investigated during the maximum set-point temperature study, with both the maximum power and internal electrical resistance values normalised with respect to their pre-cycling values. The characteristics of the modules pre- and post-cycling are summarised in Table 5. The *ZT* values for the TEG samples before the initiation of thermal cycling were in line with TEGs 1—6. As in the single set-point temperature investigation, all modules experienced a sudden 'breakdown' in performance after varying number of cycles, with significant reductions in the maximum generated power as illustrated in Fig. 5(a). The occurrence of this decreased output did not appear to correlate with the maximum temperature applied to the modules. The power reduction of TEG 7 and TEG 8, both cycled to a maximum temperature of 170 °C, was observed after 250 cycles, in comparison to after 400 cycles for TEG 11, which experienced a greater hot side temperature of 190 °C. Furthermore, the generated power of

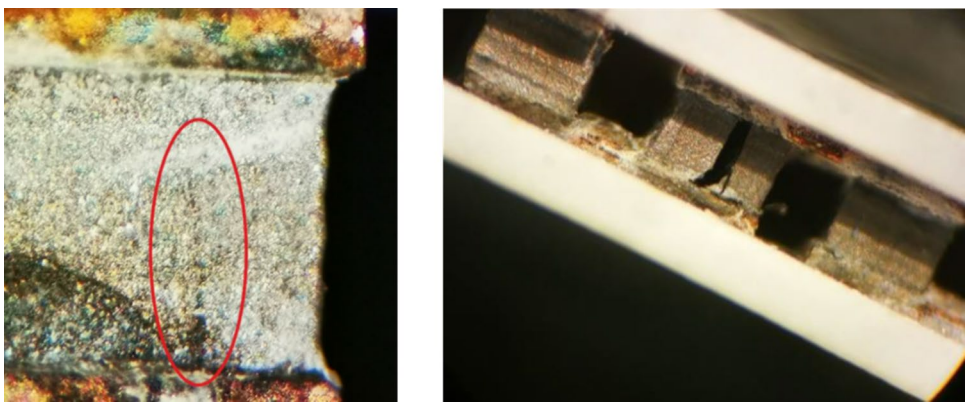

Fig. 4 Microscopic images of thermoelement legs post-thermal cycling, illustrating the presence of a crack in TEG 5 leg (left) and the through-thickness failure of a TEG 6 leg (right)

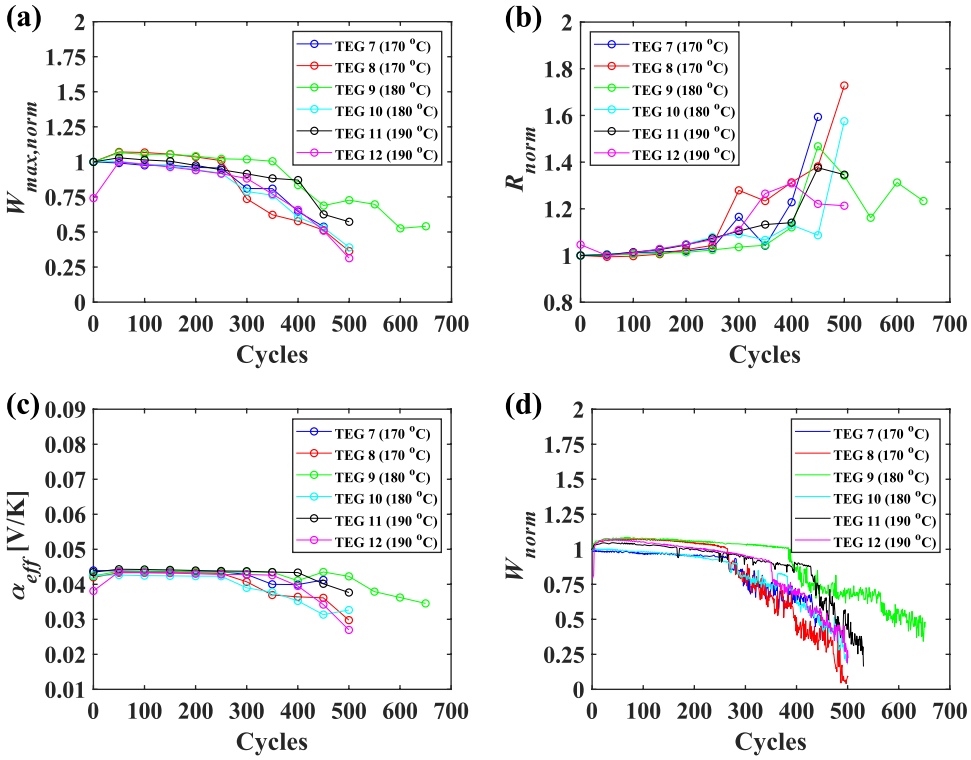

Fig. 5 Performance of all TEG samples from the maximum set-point temperature investigation characterisation tests including (**a**) normalised maximum output power (**b**) normalised internal electrical resistance (**c**) effective Seebeck coefficient and (**d**) normalised output power from the thermal cycling test

the modules subjected to a hot side temperature of 180 °C, *i.e.*, TEG 9 and TEG 10, dropped after 350 and 250 cycles respectively.

The rate of performance deterioration post-'breakdown' appears to be affected by the set-point temperature, with more rapid degradation observed for higher set-point temperatures. TEG 7's generated power remained above the 50% output threshold for a further 200 cycles, while thermal cycling ceased after only 100 additional cycles for TEG 11 with a 30% decrease in output power across these cycles. This increased degradation rate is further evident in the modules' normalised power outputs during thermal cycling, as presented in Fig. 5(d). These observations are in line with the findings of Ding et al. [17], in which greater performance deterioration was observed for modules operated closer to their maximum operating temperature. Due to the application of insufficient clamping pressure on TEG 12 at the beginning of testing, reduced output properties were determined as a result of high thermal contact resistance. Upon correction of the clamping pressure after 50 cycles, the module's properties were in line with the other samples investigated. The 'breakdown' event for this sample was found to occur after 300 cycles.

The sharp increase in internal resistance for all modules as illustrated in Fig. 5(b) corresponded to the occurrence of their individual 'breakdown' events, indicative of material degradation at the contact interface. The greatest increase in post-cycling resistance of 73% was experienced by TEG 8; in comparison, TEG 11 exhibited a resistance increase of 35%, despite being subjected to the highest set-point temperature. The average effective Seebeck coefficient (Fig. 5(c)) remained constant during

Table 5 Characteristics of the TEG samples investigated for the maximum set-point temperature investigation. Maximum uncertainties for each parameter are presented

	Pre-cycling					Post-cycling		
	V_{OC} [V] ±0.02%	α_{eff} [V/K] ±0.17%	R_{pre} [Ω] ±1.2%	W_{max} [W] ±1.1%	ZT_{pre} ±1.4%	ZT_{post} ±1.4%	$ZT_{decrease}$	R_{post} [Ω] ±1.2%
TEG 7	6.37	0.0439	2.24	4.55	0.594	0.478	20%	3.56
TEG 8	6.09	0.0420	2.09	4.45	0.591	0.368	38%	3.61
TEG 9	6.57	0.0424	2.25	4.81	0.580	0.254	56%	2.78
TEG 10	6.60	0.0426	2.10	5.16	0.584	0.326	44%	3.31
TEG 11	7.17	0.0435	2.28	5.65	0.596	0.399	33%	3.07
TEG 12	6.29	0.0381	2.26	4.39	0.596	0.287	52%	2.62

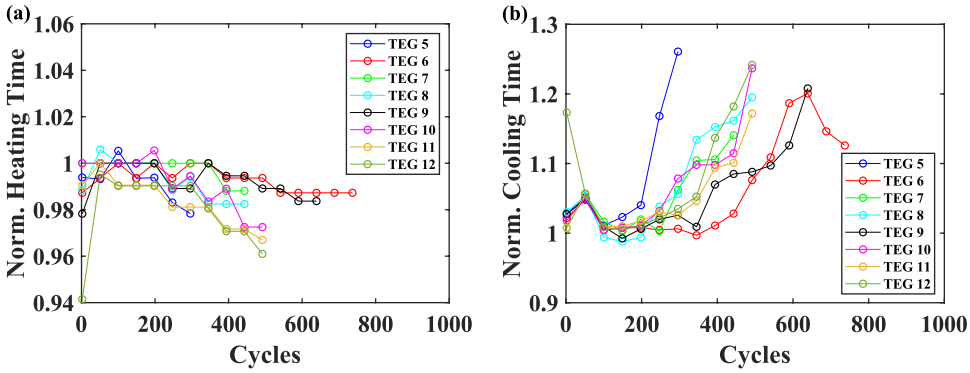

Fig. 6 Thermal cycling (**a**) heating times and (**b**) cooling times for TEGs, normalised by the heating/cooling time for the fiftieth thermal cycle. Two TEG samples for each hot side set-point temperature are presented

the initial period of thermal cycling, before decreasing in response to module deterioration as a reduced open circuit voltage was generated across the terminals. Examining the post-cycling dimensionless figure of merit values, the largest decrease was observed for TEG 9, which may have been expected due to its subjection to the greatest number of thermal cycles. For the samples which underwent 500 cycles, TEG 12, subjected to the highest set-point temperature, experienced a decrease in *ZT* of 52%, indicating the deleterious effect of thermal cycling at elevated temperatures.

4.3 Analysis of heating and cooling times

The heating and cooling times for the thermal cycle profiles investigated in the study are presented in Fig. 6 at 50 cycle intervals. As the heating time for the first thermal cycle is longer due to heating from ambient conditions, the times are normalised to those measured at the fiftieth cycle. Two datasets are shown for each maximum set-point temperature. There is a general decrease in the heating time with an increase in the number of thermal cycles, indicating that the TEG presents a larger thermal resistance to heat throughput, and therefore a shorter period of time is required to reach the desired set-point hot side temperature. The cooling times increase as it becomes more difficult to extract the heat through the sample. This is indicative of a decrease of thermal conductivity of the TEG, likely brought about by material degradation and structural deterioration such as that shown in Fig. 4. Both the heating and cooling times show the greatest change after the 'breakdown' has occurred, which reinforces the belief that the TEG fails through internal damage. Wang et al. [8] predicts that interface damage growth can be divided into three stages: (i) microcracks grow and nucleate into macrocracks, (ii) macrocracks propagate and cause interface delamination, and (iii) delamination leads to structural failure.

5 Conclusion

The performance characteristics of 12 thermoelectric generator (TEG) modules of nominally identical properties under thermal cycling conditions was experimentally investigated. For 6 samples, the cold side temperature was fixed at 30 °C while the hot side was cycled between 50 °C and 165 °C, with an average heating time (rate) of 154 s (0.75 °C/s). For a further 6 samples, the cold side temperature was fixed at 25 °C and the hot side temperature was varied from 50 °C to set-points of 170 °C, 180 °C and 190 °C, corresponding to average heating times (rates) of 169 s (0.71 °C/s), 182 s (0.71 °C/s) and 205 s (0.68 °C/s) respectively.

Performance degradation of all samples was observed with an increasing number of thermal cycles, with maximum output power reductions between 36% and 72% in combination with increased internal electrical resistances of 16% to 73%. The output power exhibited a sudden, significant decrease or 'breakdown' consistent with the findings of previous studies, which occurred at cycle numbers which varied between samples. Furthermore, the heating times were observed to decrease with an increasing number of thermal cycles, while the cooling times increased. This is attributed to a decrease in effective thermal conductivity of the TEG samples. This degradation in performance was attributed to the formation of micro-cracks at the interface of the p-n thermocouples and the conductive material to which they are attached. Microscope imaging identified evidence of damage to multiple samples. This separation equates to significant internal structural damage of the TEGs. While no correlation was found between the occurrence of these significant degradation events and the magnitude of the maximum cycle set-point temperature, more rapid performance deterioration was observed post-'breakdown' for those samples exposed to the higher set-point temperatures. In such cases, the temperature gradients through the semiconductor pellets of the TEG are the largest. The somewhat stochastic nature of the point of 'breakdown' suggests that existing intrinsic material and/or structural defects in the samples, perhaps resulting from the

manufacturing processes, play a significant role in determining the lifespan of TEGs. However, additional study of TEG module performance under thermal cycling, and post-breakdown material and structural analysis, is required to better determine this relationship.

6 Outlook

The results of this study and future studies will inform the development of a numerical finite element model to elucidate greater understanding of the 'breakdown' phenomenon and associated material degradation. It is hoped that this tool could be used to predict real life performance of TEGs. Future experimental work will focus on accurate and precise measurement of the applied pressure during thermal cycling, the use of strain gauges on the ceramic surfaces, and non-invasive visual inspection of the TEG peripheral thermocouple legs during cycling using a high-speed microscope camera. Additionally, a larger number of TEG samples from different manufacturers will be tested so that destructive inspection methods such as scanning electron microscopy (SEM) can be performed at more regular cycle intervals to determine the onset of degradation.

Acknowledgements The corresponding author wishes to acknowledge the ongoing financial support from The University of Dublin, Trinity College Provost's PhD Project Award. The authors wish to acknowledge Mr Gareth McCauley who assisted with the imaging of the samples.

Author contributions The conception and design of the study are attributed to D. Trimble and S. M. O'Shaughnessy. Data collection and analysis was performed by J. Power and N. P. Williams. The first draft of the manuscript was prepared by N. P. Williams and all authors contributed to the review of previous versions of the manuscript. The final manuscript was read and approved by all authors.

Funding Open Access funding provided by the IReL Consortium. The authors declare that no specific grants or funds were received to assist with the preparation of this manuscript.

Declarations

Competing interests On behalf of all authors, the corresponding author states that there is no conflict of interest.

References

1. Liu X, Li C, Deng YD, Su CQ (2015) An energy-harvesting system using thermoelectric power generation for automotive application. Int J Electr Power Energy Syst 67:510–516. https://doi.org/10.1016/j.ijepes.2014.12.045
2. Champier D (2017) Thermoelectric generators: A review of applications. Energy Convers Manage 140:167–181. https://doi.org/10.1016/j.enconman.2017.02.070
3. Deasy MJ, O'Shaughnessy SM, Archer L, Robinson AJ (2018) Electricity generation from a biomass cookstove with MPPT power management and passive liquid cooling. Energy Sustain Dev 43:162–172. https://doi.org/10.1016/j.esd.2018.01.004
4. Masoumi S, O'Shaughnessy S, Pakdel A (2022) Organic-based flexible thermoelectric generators: From materials to devices. Nano Energy 92:106774. https://doi.org/10.1016/j.nanoen.2021.106774
5. Al-Merbati AS, Yilbas BS, Sahin AZ (2014) A model study for cyclic thermal loading and thermal performance of a thermoelectric generator. Int J of Energy Research 38:1351–1360. https://doi.org/10.1002/er.3152
6. Fergus JW, Yerkes K, Yost K (2014) Numerical Modeling of Multimaterial Thermoelectric Devices Under Static and Cyclic Thermal Loading. J Electronic Mater 43:393–403. https://doi.org/10.1007/s11664-013-2858-7
7. Tachibana M, Fang J (2012) An Estimation of Thermal Stress of Thermoelectric Devices in the Temperature Cycling Test. Procedia Eng 27:177–185. https://doi.org/10.1016/j.proeng.2011.12.441
8. Wang P, Li JE, Wang BL, Shimada T, Hirakata H, Zhang C (2019) Lifetime prediction of thermoelectric devices under thermal cycling. J Power Sources 437:226861. https://doi.org/10.1016/j.jpowsour.2019.226861
9. Hori Y, Kusano D, Ito T and Izumi K (1999) Analysis on thermo-mechanical stress of thermoelectric module. 18th International Conference on Thermoelectrics (IEEE). pp 328–331. https://doi.org/10.1109/ICT.1999.843396
10. Hatzikraniotis E, Zorbas KT, Samaras I, Kyratsi T, Paraskevopoulos KM (2010) Efficiency Study of a Commercial Thermoelectric Power Generator (TEG) Under Thermal Cycling. J Electron Mater 39:2112–2116. https://doi.org/10.1007/s11664-009-0988-8
11. de Cerqueira Veras JC, Vieira DA, Melo EC, de Souza CP (2015) An automatic thermal cycling based test platform for thermoelectric generator testing. 2015 IEEE International Instrumentation and Measurement Technology Conference (I2MTC). pp 1949–1953. https://doi.org/10.1109/I2MTC.2015.7151580
12. Barako MT, Park W, Marconnet AM, Asheghi M, Goodson KE (2012) A reliability study with infrared imaging of thermoelectric modules under thermal cycling. 13th Intersociety Conference on Thermal and Thermomechanical Phenomena in Electronic Systems (IEEE). pp 86–92. https://doi.org/10.1109/ITHERM.2012.6231417
13. Barako MT, Park W, Marconnet AM, Asheghi M, Goodson KE (2013) Thermal Cycling, Mechanical Degradation, and the Effective Figure of Merit of a Thermoelectric Module. J Electron Mater 42:372–381. https://doi.org/10.1007/s11664-012-2366-1
14. Tatarinov D, Wallig D, Bastian G (2012) Optimized Characterization of Thermoelectric Generators for Automotive Application. J Electron Mater 41:1706–1712. https://doi.org/10.1007/s11664-012-2040-7

15. Park W, Barako MT, Marconnet AM, Asheghi M, Goodson KE (2012) Effect of thermal cycling on commercial thermoelectric modules. 13th Intersociety Conference on Thermal and Thermomechanical Phenomena in Electronic Systems (IEEE). pp 107–112. https://doi.org/10.1109/ITHERM.2012.6231420
16. Tenorio HCRL, Vieira DA, Souza CPD (2017) Measurement of parameters and degradation of thermoelectric modules. IEEE Instrum Meas Mag 20:13–19. https://doi.org/10.1109/MIM.2017.7919127
17. Ding LC, Akbarzadeh A, Date A (2016) Performance and reliability of commercially available thermoelectric cells for power generation. Appl Therm Eng 102:548–556. https://doi.org/10.1016/j.applthermaleng.2016.04.001
18. Merienne R, Lynn J, McSweeney E, O'Shaughnessy SM (2019) Thermal cycling of thermoelectric generators: The effect of heating rate. Appl Energy 237:671–681. https://doi.org/10.1016/j.apenergy.2019.01.041
19. Harish S, Sivaprahasam D, Jayachandran B, Gopalan R, Sundararajan G (2021) Performance of bismuth telluride modules under thermal cycling in an automotive exhaust thermoelectric generator. Energy Convers Manag 232:113900. https://doi.org/10.1016/j.enconman.2021.113900
20. Ziolkowski P, Blaschkewitz P, Müller E (2021) Validation of commercial Bi2Te3-based thermoelectric generator modules for application as metrological reference samples. Measurement 177:109247. https://doi.org/10.1016/j.measurement.2021.109247
21. Riyadi TWB, Utomo BR, Effendy M, Wijayanta AT, Al-Kayiem HH (2022) Effect of thermal cycling with various heating rates on the performance of thermoelectric modules. Int J Therm Sci 178:107601. https://doi.org/10.1016/j.ijthermalsci.2022.107601
22. Mirhosseini M, Rezania A, Rosendahl L, Iversen BB (2017) Effect of Thermal Cycling on Zinc Antimonide Thin Film Thermoelectric Characteristics. Energy Procedia 142:519–524. https://doi.org/10.1016/j.egypro.2017.12.081
23. Brostow W et al (2012) Bismuth telluride-based thermoelectric materials: Coatings as protection against thermal cycling effects. J Mater Res 27:2930–2936. https://doi.org/10.1557/jmr.2012.335
24. Gao Y et al (2010) Nanostructured Interfaces for Thermoelectrics. J Electronic Mater 39:1456–1462. https://doi.org/10.1007/s11664-010-1256-7
25. Williams NP, Roumen L, McCauley G, O'Shaughnessy SM (2021) Performance evaluation of thermoelectric generators under cyclic heating. J Phys: Conf Ser 2116:012087. https://doi.org/10.1088/1742-6596/2116/1/012087
26. Hodes M (2005) On one-dimensional analysis of thermoelectric modules (TEMs). IEEE Trans Compon Packag Technol 28:218–229. https://doi.org/10.1109/TCAPT.2005.848532
27. Huang K, Yan Y, Wang G, Li B (2021) Improving transient performance of thermoelectric generator by integrating phase change material. Energy 219:119648. https://doi.org/10.1016/j.energy.2020.119648
28. Jacquot A, Jaegle M, König J, Ebling D, Böttner H (2007) Theoretical study of the Harman method for evaluating the thermoelectric performance of materials and components at high temperature. Proceedings of the 5th European Conference on Thermoelectrics. Odessa, Ukraine
29. Hsu CT, Huang GY, Chu HS, Yu B, Yao DJ (2011) An effective Seebeck coefficient obtained by experimental results of a thermoelectric generator module. Appl Energy 88:5173–5179. https://doi.org/10.1016/j.apenergy.2011.07.033